Thin–Walled Structures 206 (2025) 112577

Contents lists available at ScienceDirect

Thin-Walled Structures

journal homepage: www.elsevier.com/locate/tws

Full length article

On the imperfection sensitivity and design of buckling critical wind turbine towers

H.N.R. Wagner [a,b,*], C. Hühne [a,c]

[a] Technical University Braunschweig, Institute of Adaptronic and Functional Integration, Langer Kamp 6 38106 Braunschweig, Germany
[b] Siemens Mobility GmbH, SMO RI R&D IXL PE, Ackerstr. 22 38126 Braunschweig, Germany
[c] German Aerospace Center (DLR), Institute for Composite Structures and Adaptive Systems, Lilienthalplatz 7 38108 Braunschweig, Germany

ARTICLE INFO

Keywords:
Wind turbine support tower
Buckling
Dimple imperfection
Reference resistance design
Finite element analysis

ABSTRACT

Wind turbine towers pose major challenges for design engineers due to their complex geometry, nonlinear material behavior and imperfection sensitivity. In service, these thin-walled shells are burdened by a combination of complex load cases and prone to buckling. In fact, one of the main design drivers of wind turbine towers is stability failure for which often the design recommendation of the EN-1993–1–6 are used.

Recently an international shell buckling exercise was caried out by the team behind the EN-1993–1–6 design standard. Within this exercise 29 teams from academia and industry were asked to perform a series of linear and non-linear finite element simulations of an 8-MW multi-strake steel wind turbine support tower segment. In general, the linear and nonlinear analyzes posed no challenge for the shell buckling experts from around the world. However, the imperfection sensitivity analysis results scattered significantly among the participants. In addition, there was little consensus as to whether the given tower design is actually safe.

The authors, whose background is aerospace engineering, participated in this exercise and show in this article how they overcome the challenges of this typical civil engineering problem. Among linear and non-linear analyzes the authors show the results of state-of-the-art shell buckling concepts which were developed for aerospace shells like interstage tanks and adapters but are also applicable to wind turbine towers.

Abbreviations and glossary

E	Elasticity modulus
EBC	Energy Barriere Criterion
Exp.	Experiment
GMNA	Geometrically and material nonlinear analysis
GMNIA	Geometrically and material nonlinear analysis with imperfections
GNA	Geometrically nonlinear analysis
GNIA	Geometrically nonlinear analysis with imperfections
ISBE	International shell buckling exercise
L	Cylinder height/length
LBA	Linear bifurcation analysis
LRSM	Localized reduced stiffness method
KDF	Knockdown factor
MNA	Material nonlinear analysis
N	Buckling load
R	Radius of a cylinder
SBPA	Single Boundary Perturbation Approach
SPLA	Single Perturbation Load Approach
t	Wall thickness
Y	Yield strength
λ	Relative shell slenderness
ρ	Knockdown factor
ν	Poisson's ratio

1. Introduction

Cylindrical shells are structural elements widely used in various engineering applications, such as aerospace [1,2] marine [3,4] and civil engineering [5,6] due to their high strength-to-weight ratio. Under axial compression, these structures can experience buckling, a critical failure mode that significantly influences their design and safety [7]. The presence of geometric imperfections further complicates the buckling behavior, necessitating sophisticated design approaches and robust analysis techniques.

* Corresponding author.
E-mail address: ro.wagner@tu-braunschweig.de (H.N.R. Wagner).

https://doi.org/10.1016/j.tws.2024.112577
Received 29 July 2024; Received in revised form 12 September 2024; Accepted 10 October 2024
Available online 18 October 2024

The buckling of cylindrical shells under axial compression is a classical problem in structural mechanics. According to classical linear buckling theory [8], this critical load N is given by (1) for pure elastic material behavior and for plastic material behavior by (2):

$$N_{elastic} = \frac{2 \cdot \pi \cdot E \cdot t^2}{\sqrt{3(1-\nu^2)}} \tag{1}$$

$$N_{plastic} = 2 \cdot \pi \cdot R \cdot t \cdot Y \tag{2}$$

where E is the elasticity modulus, t is the wall thickness of the cylinder, n the Poisson's ratio, R the cylinder radius and Y the yield stress.

However, real-world shells invariably contain imperfections that lower the buckling load significantly below this theoretical value. Cylindrical shells are highly sensitive to imperfections, which can be in the form of initial geometric deviations [9], material inconsistencies [10], or boundary condition irregularities [11]. These imperfections can cause the actual buckling load to be a small fraction of the theoretical critical load. This sensitivity was first noted by Koiter [12] who demonstrated that even minor imperfections could lead to substantial reductions in buckling strength.

The traditional approach [13] to account for imperfections in the design of cylindrical shells involves the use of empirical knockdown factors (3) which are multiplied with the reference buckling load of a shell.

$$\rho_{exp} = \frac{N_{exp}}{N_{reference}} \tag{3}$$

These factors are derived from experimental data and provide a safety margin by reducing the theoretical buckling load. Historically, NASA SP-8007 [14] has been a key reference, providing conservative knockdown factors for different shell geometries and loading conditions. These factors are typically expressed as a function of shell geometry (R/t ratio – Radius-to-thickness ratio) and material properties.

$$\rho \; = 1 - 0.902 \cdot \left(1 - e^{-\left(\frac{1}{16}\sqrt{\frac{R}{t}}\right)}\right) \tag{4}$$

Recent advances have focused on refining knockdown factors through improved understanding of imperfection patterns and distributions [15]. Computational methods, such as finite element analysis (FEA) [16], have enabled more accurate predictions of the influence of imperfections on buckling loads. Research has also explored probabilistic approaches [17] to account for variability in imperfections [18], leading to the development of stochastic knockdown factors [19,20].

Finite Element Analysis has become a cornerstone in the analysis of cylindrical shells under axial compression. Modern FEA software allows for detailed modeling of imperfections [21] and provides insights into their effects on buckling behavior [22].

Advanced modeling techniques, such as incorporating realistic imperfection shapes based on measured data [23] or statistical distributions enhances the accuracy of numerical predictions [24].

Experimental testing remains essential for validating theoretical and numerical predictions [25]. Laboratory tests on cylindrical shells involve precisely controlled axial compression to observe buckling behavior and post-buckling response [26]. High-resolution measurement techniques, such as digital image correlation (DIC), allow for detailed tracking of deformations and imperfection patterns [27].

Experimental results are used to calibrate and validate numerical models [28]. A key aspect of this correlation is the accurate representation of initial imperfections in the models [29]. By comparing experimental and numerical buckling loads and deformation patterns [30], researchers can refine their models and improve the predictive capability of numerical methods [31].

Cylindrical shells are usually tested with fully clamped boundary conditions [32] and there is an increasing number of publications which study different kind of boundary conditions for cylindrical shells like localized multi-region boundary conditions [33] which occur in steel silo [34]. Detailed numerical and experimental studies for this specific type of boundary conditions were led by Jiao et al. [35,36].

Scaling effects are important in experimental studies of cylindrical shells [37]. Smaller-scale models are often used in laboratory settings, but these may not replicate the behavior of full-scale structures due to differences in material properties and imperfection magnitudes [38].

The use of advanced materials, such as composites, introduces new challenges and opportunities in the design of cylindrical shells [39]. These materials offer improved performance but require novel analysis techniques to account for their complex behaviors under axial compression [40].

In addition to realistic measured geometric imperfections, there is also a considerable amount of work put in researching artificial geometric imperfections [41,42]. The aim was to determine a "worst" imperfection which leads to a design lower-bound for the buckling load of cylindrical shells. The shape which can be a categorized as worst imperfection is according to Horak et al. [43] the "dimple" imperfection. The first concept which uses a dimple and determine a corresponding design load by adjusting the amplitude of the dimple is the single perturbation load approach (SPLA) by Hühne et al. [44]. The SPLA has been investigated by a large number of researchers during the DESCIOS project [45]. In the years following the publication of the SPLA different similar "dimple" design concepts have been developed. The worst multiple perturbation load approach (WMPLA [46]) uses an optimization algorithm [47] to determine position and amplitude of dimple imperfections which lead to an improved design load compared to the regular SPLA. The single boundary perturbation approach (SBPA) induces a single dimple by means of an edge perturbation [48,49]. The localized reduced stiffness method (LRSM) [50,51] induces a dimple by means of a local reduction of the membrane stiffness of a shell and is based on the original reduced stiffness method (RSM) by Croll et al. [52,53].

The SPLA and LRSM type of methods have so far only been applied to aerospace or marine shell structures [54,55]. In 2022 a shell buckling "round-robin" exercise took place where different authors form the world were invited to perform imperfection sensitivity analyze to an civil engineering type shell, a wind turbine tower. This article summarizes the results of the shell buckling exercise and the application of state-of-the-art dimple imperfection concepts which are used to analyze the wind turbine tower.

This article is structured as follows, the main results of international shell buckling exercise and its challenging task are presented in chapter 2. The state-of-the-art dimple imperfection concepts are presented in chapter 3 and validated by means of a well-documented test series of isotropic cylinders. In chapter 4, the wind turbine tower shell is presented is analyzed using the methods presented in chapter 3. In the last 5th chapter, important findings are summarized and discussed. An outlook for future research is given.

2. The international shell buckling exercise

The international shell buckling exercise (ISBE) took place in 2022 from about May to October and was initiated by Adam Sadowski from the Imperial college of London and Marc Seidel from Siemens Gamesa [56,5]. In total 29 research groups from around the world were given a shell buckling problem which should be analyzed with either FEA or analytical methods (or both). The main task of the ISBE was to perform a series of simulations to evaluate the linear and nonlinear stability and material strength behavior of a wind turbine tower with 2 two load cases (LC1 and LC2). The analyzes were performed in accordance with the Eurocode standard. The following analyzes should be performed:

1. LBA – linear bifurcation analysis

2. MNA – material nonlinear analysis
3. GNA – geometrically nonlinear analysis
4. GMNA – geometrically and material nonlinear analysis
5. GMNIA – geometrically and material nonlinear analysis with imperfections

The results of the first four analysis types (LBA, MNA, GNA and GNMA) were in general in good agreement among the different research groups. Significant differences however were determined for the results of the GMNIA, see Fig. 1. Most research groups applied eigenmode imperfections (64 %), about 23 % of the research groups applied weld imperfections, the remaining research groups applied for example superpositions of multiple LBA eigenmodes and only one research group (the authors of this article) applied dimple imperfection principles. Another interesting result of the ISBE is that nearly half of all GMNIA submission concluded that the tower design loads are not safe as the LPF is below one.

The ISBE was a good opportunity for the authors to apply the relatively new dimple imperfection concepts to a civil engineering shell. There were several challenges for the application of the EBC/SPLA to the wind turbine tower because the dimple concepts were mainly developed and tested to aerospace shells (interstage, adapter and tanks). The main challenges were:

1. The tower is under a combination of multiple different loads and not only loaded with one load case (axial compression, bending, shear, torsion…).
2. The tower has a relatively low yield strength and therefore plastic buckling is relevant compared to a pure elastic buckling problem.
3. The tower is only fixed (in terms of mechanical boundary conditions) at the bottom end and not on the top end.
4. The tower has different wall thickness values along its height and is a cylindrical-conical-cylindrical shell.

Unfortunately, no experimental buckling test data exist for the wind turbine tower as a benchmark. Due to the associated costs for manufacturing and testing, full-scale buckling tests are rare. The curious reader can find a pretty good description of a buckling test of a full-scale launch vehicle shell in [57] by Hao et al.

3. Analysis of an isotropic cylinder under axial compression

In this chapter, state-of-the-art shell buckling design concepts with regard to imperfections are explored, laying the groundwork for more complex analyses ahead in chapter 4. A simple example of a cylindrical shell under uniform axial compression is presented and validated with experimental data and verified with analytical equations as well as numerical methods. By observing the model's response to various imperfections concepts, fundamental principles of shell buckling behavior are illustrated.

3.1. Benchmark geometry and finite element model

The shell presented in this section is an unstiffened isotropic steel shell (seamless beer can) which was investigated by Verduyn et al. [58]. The corresponding material and geometry properties are given in Table 1. The whole test series consisted of 33 nominal identical test specimens and is therefore well suited to validate numerical design approaches.

The IW1 shells were modeled by using linear shell elements (S4R in ABAQUS [59]) and the finite element length (see Fig. 2) was defined as 0.92 mm according to $0.5\sqrt{Rt}$ [16]. The mechanical boundary conditions on both cylinder edges are defined as clamped by using rigid-body interactions (Tie) which are coupled with a reference point. The displacement in axial direction is free at the top cylinder edge for load application.

The load-displacement curve of the perfect shell IW1 according to a GNA using ABAQUS is shown in Fig. 3, a summary of the corresponding buckling loads is given in Table 2.

3.2. Application of numerical shell buckling design concepts to the cylinder

Geometric imperfections have a significant influence on the buckling load of structural elements. The primary reasons for the reduction in buckling load due to these imperfections are as follows:

Table 1
Geometry and material data for the cylindrical shells after [58].

Material parameter	Shells IW1
elasticity modulus E	208,000 N/mm^2
Poisson's ratio v	0.3
Yield Stress	450 N/mm^2
Geometry parameter	
Radius R	33 mm
Free Length L	100 mm
Wall thickness t	0.1 mm
R/t	330
L/R	3
Z	2890

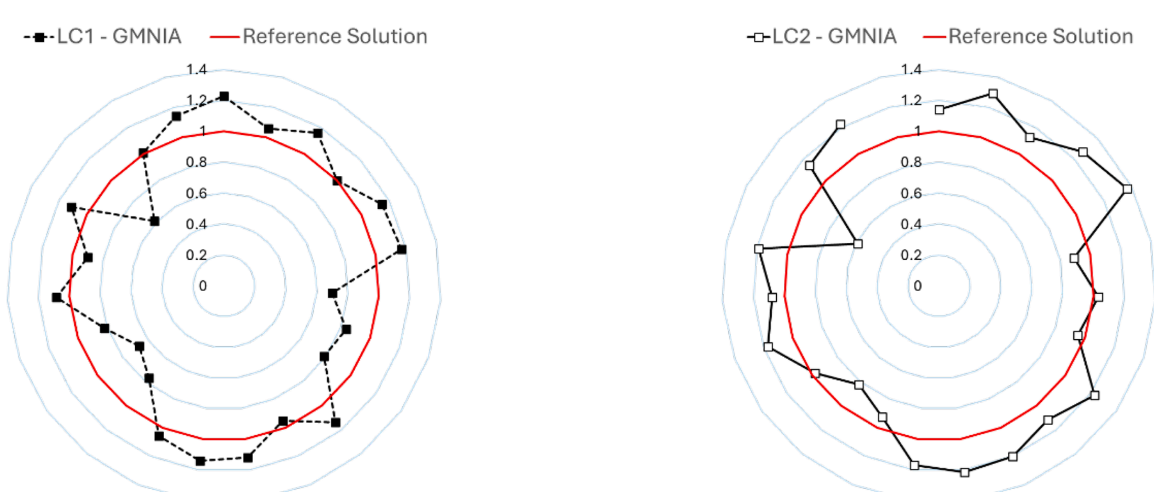

Fig. 1. Scatter of the GMNIA solutions for the wind turbine tower LC1 (left) LC2 (right) reproduced from [56].

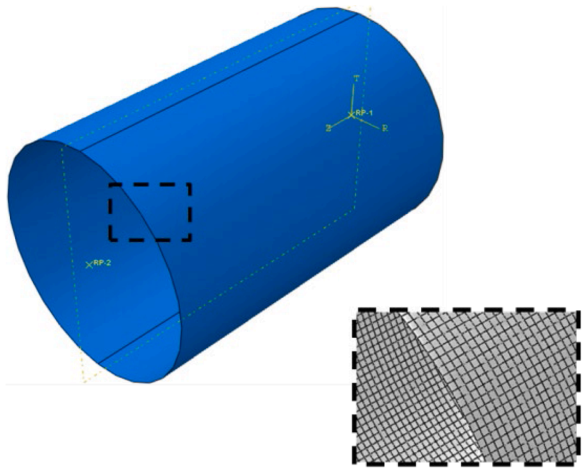

Fig. 2. CAD model of the IW1 shells with mesh and reference points for boundary condition and load application.

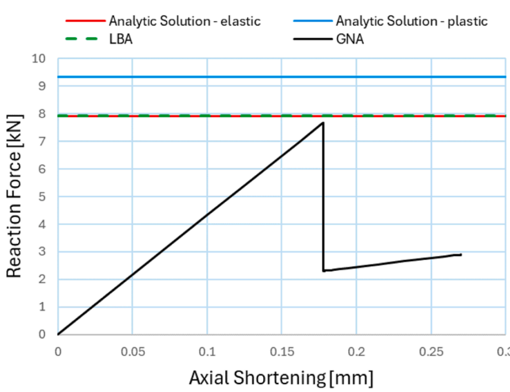

Fig. 3. Load Displacement curve of the IW1 shell according to GNA and results from LBA and analytical equations.

Table 2
Buckling loads of the IW1 shells.

LBA	GNA	Analytical					
7.90	7.66	7.90					
Shell	N_{exp}	Shell	N_{exp}	Shell	N_{exp}	Shell	N_{exp}
IW1–16	3.05	IW1–24	4.27	IW1–33	4.03	IW1–42	3.82
IW1–17	3.53	IW1–26	3.99	IW1–34	4.68	IW1–43	3.83
IW1–18	4.5	IW1–27	4.16	IW1–36	4.43	IW1–44	4.23
IW1–19	4.51	IW1–28	4.24	IW1–37	3.55	IW1–45	3.99
IW1–20	3.89	IW1–29	4.49	IW1–38	4.2	IW1–46	3.35
IW1–21	4.01	IW1–30	4.46	IW1–39	4	IW1–47	3.51
IW1–22	3.82	IW1–31	4.47	IW1–40	4.08	IW1–48	3.43
IW1–23	4.5	IW1–32	4.01	IW1–41	4.03	IW1–49	3.48
						IW1–50	3.93

1. **Initial Deformations**: Imperfections such as initial out-of-straightness or out-of-roundness result in pre-existing deformations in the structure. These initial deformations mean the structure is already closer to its buckling shape before any external load is applied, requiring a smaller additional load to reach the critical buckling condition.
2. **Stress Concentrations**: Imperfections lead to localized stress concentrations, where certain regions of the material experience higher stresses than in a perfect structure. These localized stresses can cause premature yielding or instability, thus reducing the overall buckling load.
3. **Load Redistribution**: Geometric imperfections cause an uneven distribution of loads. In an ideal, perfectly symmetrical structure, the load is distributed evenly. However, imperfections cause some areas to carry more load than others, leading to earlier buckling in the more heavily loaded regions.

In summary, geometric imperfections reduce the buckling load due to the creation of initial deformations, stress concentrations, uneven load distributions, and nonlinear behavior, thereby making the structure less stable under compressive loads.

The initial measured geometric imperfections (MGI) of the IW1 shells have been measured and documented in form of Fourier coefficients which are used for a double Fourier series in order to apply the imperfect shell geometry to the mesh of the ABAQUS FEA model. The imperfection pattern leading to the highest (IW1–33 – 26 %) and lowest (IW1–30 – 15 %) buckling load reduction are shown in Fig. 4.

A detailed comparison of the experimental results of the IW1 shells with the numerical analysis using ABAQUS is shown in Fig. 5. The MGI were considered using a GNIA in ABAQUS, however, the average buckling load reduction due to MGI is only 20 % whereas the average buckling load reduction in the experimental results is about 50 %.

A design concept for thin-walled shells which is independent of imperfection measurements and based on the single dimple is the SPLA by Hühne [44]. Within the framework of the SPLA a single dimple is caused in a thin-walled shell by means of a lateral perturbation load. The buckling load is then determined with respect to the amplitude of the perturbation load (or depth of the dimple) and for multiple calculations with increasing amplitude of the perturbation load a characteristic lower-bound diagram can be determined.

The characteristic lower-bound diagram is shown in Fig. 6 (left). This diagram has in general 4 sections for axial compression. In the first section the “perfect” buckling load N_0 is constant because the “imperfection” is too small and the influence is negligible. In the second section, a linear reduction of the buckling moment occurs. The third section is characterized by local and subsequent global buckling (also known as snap-through buckling [60,61]). Local buckling is the sudden formation of a dimple on the cylinder surface (the shell surface snaps inwards) which is accompanied by a stiffness degradation of the load displacement curve as shown in Fig. 6 (right). In numerical simulations with for example artificial dampening the load can still be increased after the local buckling event occurred until the buckles globally. The buckling load N_1 corresponds to the global buckling load values in Section 3 and 4 as shown in Fig. 6 (right). The global buckling load is not sensitive to a further increase of the perturbation load (or increase of the dimple amplitude) and remains rather constant. This plateau behavior of the buckling load is also known as lower-bound of the buckling load [62, 63]. The buckling load of a shell is independent from further increasing local imperfections because the membrane stresses are zero in this region [50]. The local buckling load, however, reduces in a linear fashion using the SPLA.

The authors of this article studied the local and global buckling event in axially compressed cylinders experimentally by inducing local buckling deliberately [64]. The experimental studies showed that local buckling leads in almost all cases to global buckling of the cylinder (meaning the load cannot be increased as shown in Fig. 6 left) but in rare cases the shell buckles locally and the load can be further increased and global buckling occurs at higher loads. For a worst-case scenario, choosing the minimum local buckling load N_{min} is necessary for safe design.

In the fourth section, the structural behavior of the cylinder changes, sudden local buckling does not occur anymore. The dimple amplitude in region 4 is so large that local buckling occurs not suddenly anymore it is rather a smooth formation of a dimple (the shell surface is already bent inwards and only the dimple amplitude increases) on the cylinder surface which leads to a more stable load carry behavior of the cylinder until global buckling and a slight degradation of the axial stiffness. A

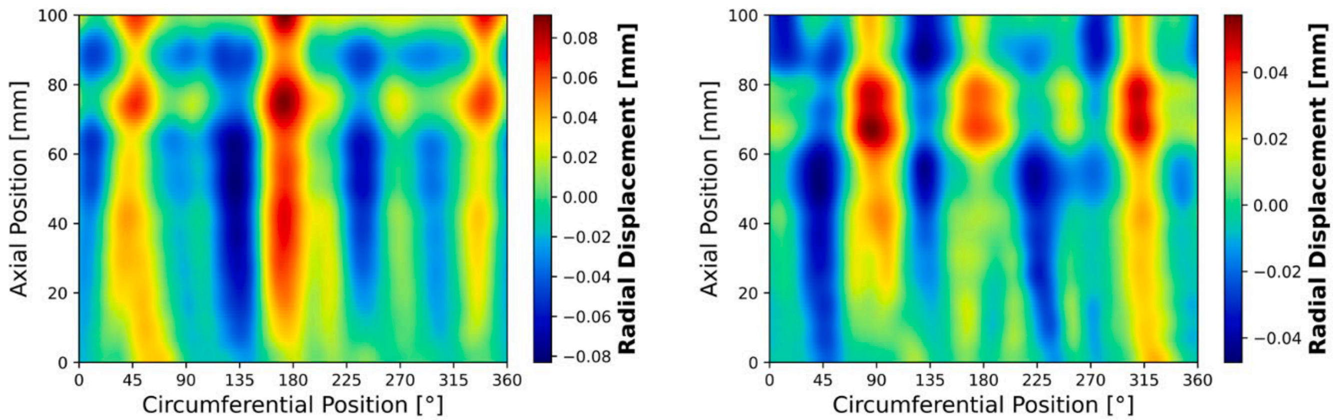

Fig. 4. MGI pattern for shell IW1–33 (left) and IW1–30 (right).

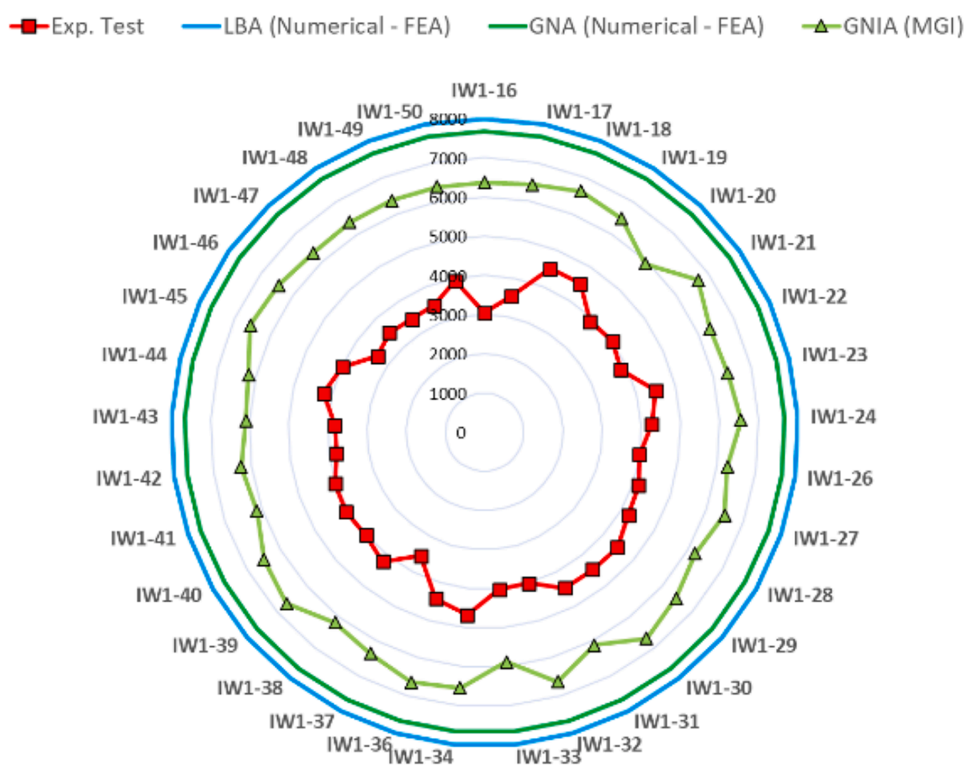

Fig. 5. Comparison of buckling loads: LBA, GNA, MGI and test data for the IW1 shells.

more detailed description of this behavior is given in [49].

In its original definition, the SPLA defined the load N_1 in the plateau range as its design load, which is in the pure elastic case 4.59 kN. However, many publications like [9] and [10] have shown that the N_1 load is often not conservative enough with respect to experimental results. A worse outcome with respect to buckling occurs if local snap-through buckling happens (from Section 3). The authors therefore recommend using the minimum local buckling load N_{min} for design purpose when using the SPLA. The minimum local buckling load according to the SPLA (for pure elastic material behavior) is for the IW1 shell series 2.74 kN as shown in Fig. 7 (left) which is conservative with respect to all experimental results.

Successor design approaches to the SPLA like the SBPA [62] (Fig. 8–right) or the LRSM [50] (Fig. 8- left) choose always the minimum local buckling load in Section 3 as a design load. The SBPA and LRSM work similar to the SPLA, they induce a single dimple by means of a localized imperfection. In case of the SBPA, an edge perturbation is used as imperfection and the LRSM used a localized reduction of the membrane stiffness (the LRSM is a further development of the reduced stiffness methods – RSM). For large, localized imperfections snap-through buckling occurs and the minimum local buckling loads can be used as design loads.

The minimum local buckling loads of the SPLA, SBPA and LRSM are shown in Fig. 12 for the elastic case and the perfect-plastic case, an interesting observation is that the minimum local buckling load is 3–10 % lower if the yield stress of 450 MPa is considered when compared to pure elastic buckling. Even the lowest experimental buckling load from IW1–16 with 3.05 kN can be approximated if the yielding is considered. This test specimen was in prior analysis always defined as an outliner, but it is assumed that imperfections occurred for this specimen which led to some kind of stress concentration in a way the premature yielding occurred hence leading to a lower-than-expected buckling load.

The yield stress for this specimen is much higher than the elastic buckling stress which would one lead to believe that this shell buckles

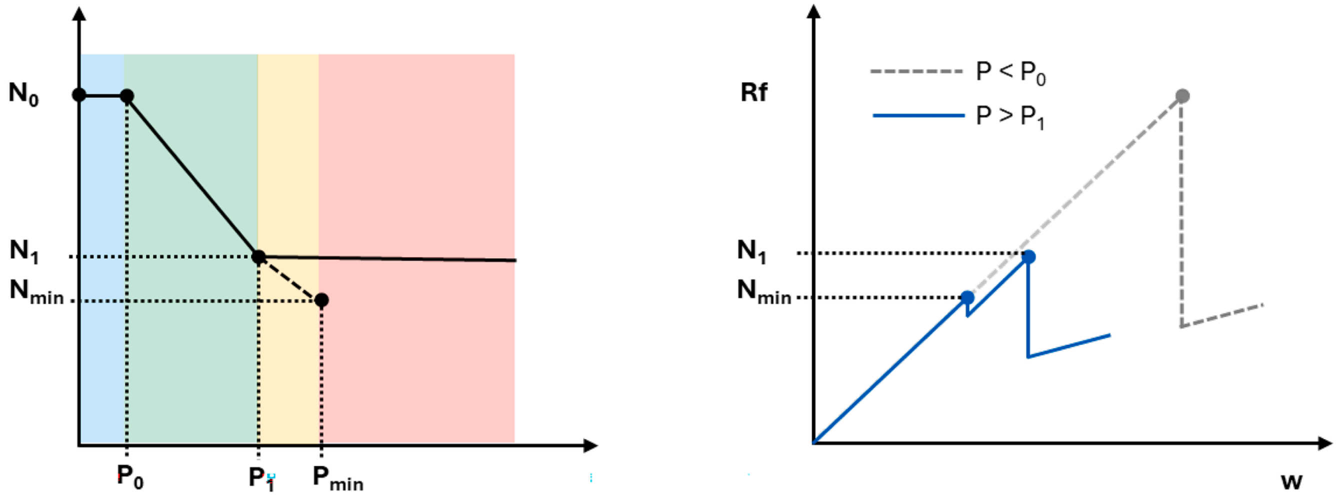

Fig. 6. Characteristic Lower-bound diagram of the SPLA (right) – corresponding reaction force – axial shortening curve (left).

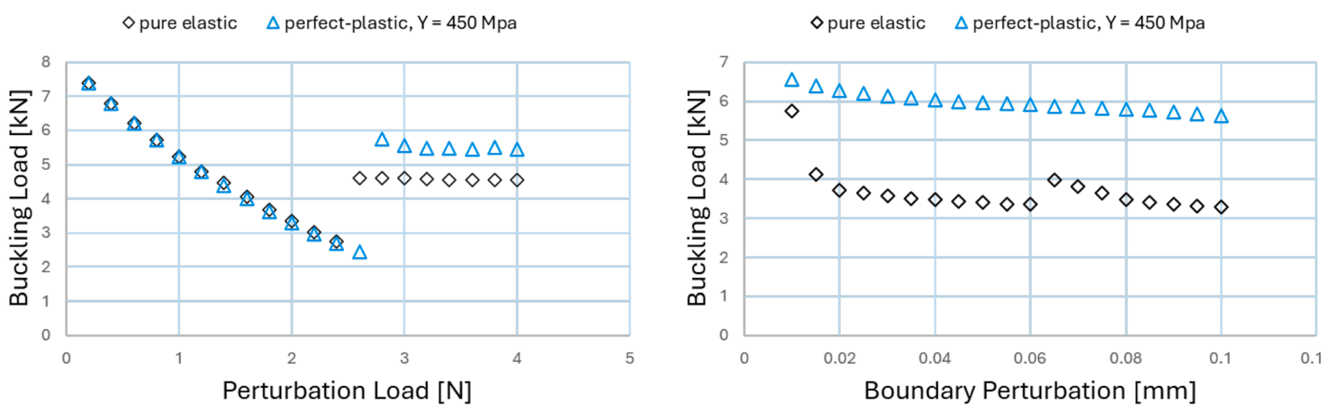

Fig. 7. SPLA (left) vs. SBPA (right).

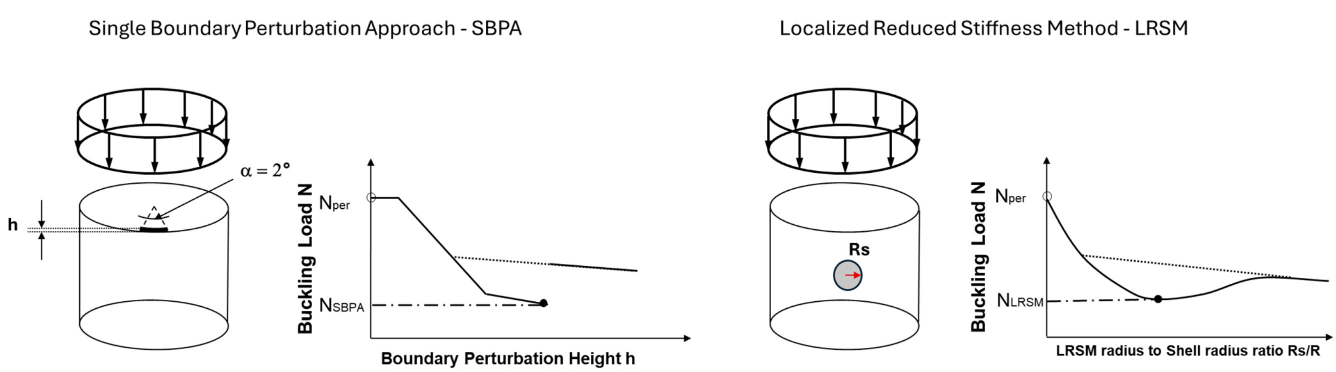

Fig. 8. Design concepts for cylinders under axial compression (SBPA and LRSM).

pure elastically. However, the definition if a shell buckles in the elastic or plastic range is still subject of research. Authors in [65] stated the shell buckle in the pure elastic range if $\lambda > \sqrt{3}$ and this shell has $\lambda \sim 1$, see Fig. 10. According to the Eurocode EN 1993–1–6 [8] definition it buckles still in the elastic range.

The SBPA (Fig. 7– right) gives much higher results if yielding is considered from 3.35 kN in the elastic case to 5.9 kN in the plastic case. This behavior is not yet understood and subject to research. But it looks like the SBPA is not suitable for the design of cylinders if yielding is relevant. The design load according to the LRSM (Fig. 9- left) equals to 3.1 kN in the pure elastic case and 3.01 kN in the perfect-plastic case.

The energy barrier criterion (EBC illustrated in Fig. 11) was also applied to the IW1 shells, this method works basically inverse to the previously presented lower-bound approaches.

Within the framework of the EBC, the shell is pre-loaded with an axial Force F which is smaller than the expected buckling load (for example 10 % of the expected buckling load which is then incrementally increased until the lower local buckling load is determined). In a subsequent second step a radial perturbation displacement is applied to the pre-loaded shell and the corresponding reaction force Rf is measured (as shown in Fig. 9- right). For axial forces which are below the lower local buckling load (design load of the EBC), the reaction force RF increases as

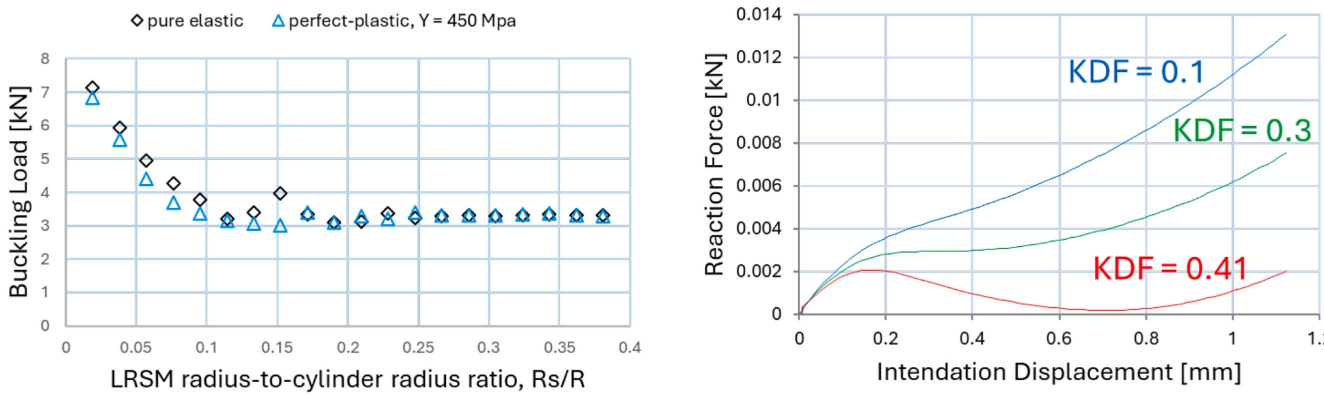

Fig. 9. LRSM (left) vs. EBC (right) – difference between pure elastic and perfect-plastic is not shown as it is very small.

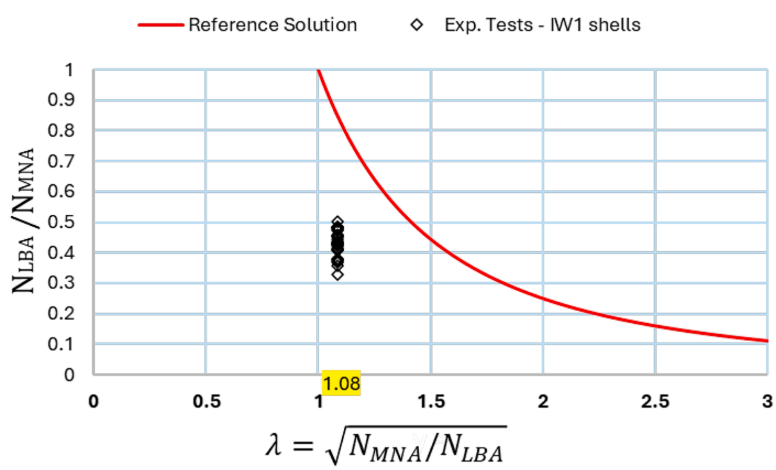

Fig. 10. Test results of the IW1 shells vs. shell slenderness parameter λ.

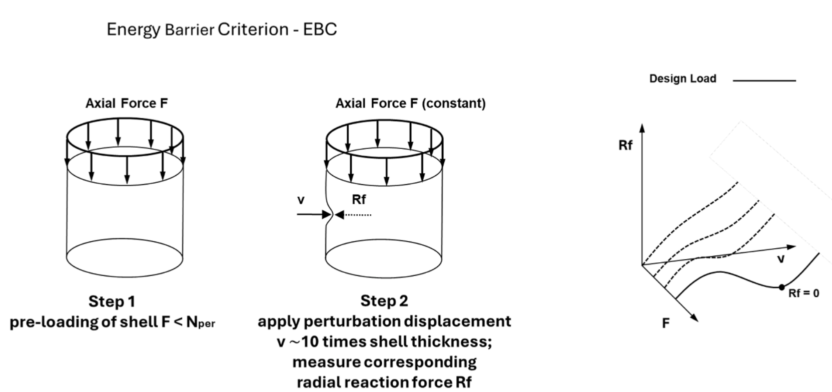

Fig. 11. Illustration of the EBC applied to a cylinder.

the perturbation displacement increases. However, as the axial force F approaches the lower local buckling load, the reaction force Rf approaches zero. This method finds basically the load level which leads to the first occurrence of local buckling. The previously presented lower-bound methods reduce the buckling load until the minimum local buckling load is found. The minimum local buckling load according to the EBC equals to 3.24 kN in the pure elastic case and 3.16 kN in the perfect-plastic case ($Y = 450$ MPa).

The main results of this section are summarized in Fig. 12 for pure elastic buckling (left) and perfect-plastic buckling (right). Overall, all lower-bound methods determine a close approximation for the lowest experimental result of the IW1 shell series. The SPLA using N_{min} is conservative in every case as is the LRSM, the EBC comes very close (difference in plastic case to lowest test result is only 3.7 %). The SBPA is conservative to nearly all test results in the pure elastic case but is not suitable for the application of shell buckling if yielding is relevant, the design load of the SBPA is with 5.9 kN far above the test results.

3.3. Application of analytical knockdown factors to the cylinder

In shell buckling design KDFs are commonly applied to cover the effect of imperfections, the most commonly applied cylinder buckling KDFs in aerospace engineering belong to the NASA SP-8007. New and less conservative design KDF have been developed by the authors of this

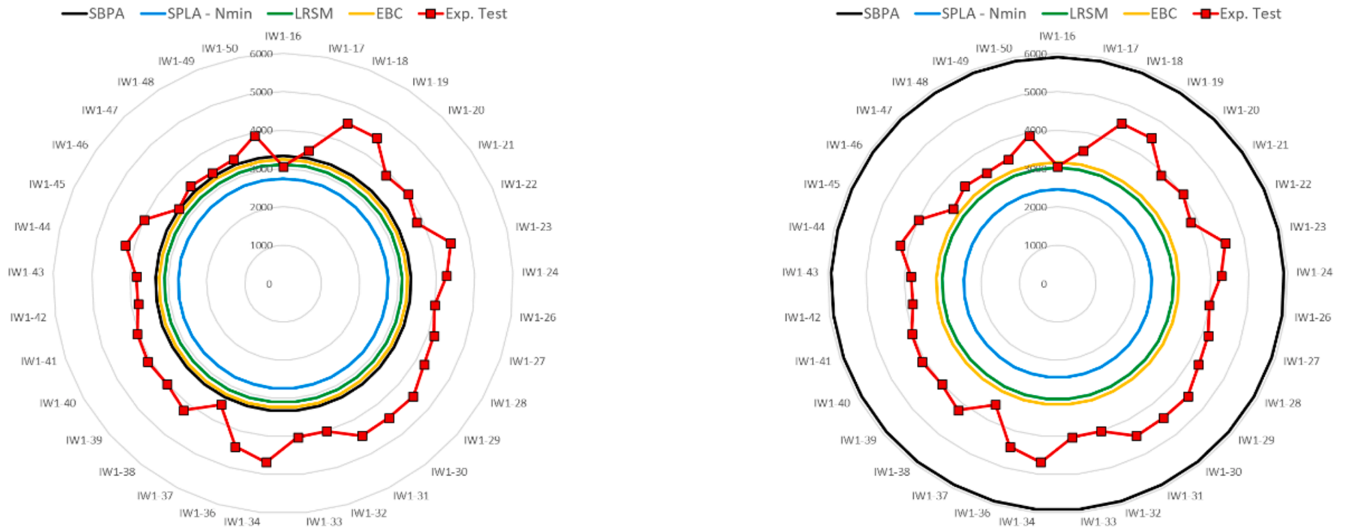

Fig. 12. Comparison of lower-bound approaches vs experiments: pure elastic (left) perfect-plastic $Y = 450$ MPa (right).

paper in [66,50] using the SBPA, LRSM and SPLA which are shown in Fig. 13 (left) for different values of the Batdorf parameter Z, see Eq. (5).

$$Z = \frac{L^2 \cdot \sqrt{(1-\nu^2)}}{R \cdot t} \tag{5}$$

Those curves are very similar for the LRSM and SBPA for $Z > 1300$ and only a slightly different for small Z ⟨ 1300. The SPLA curve for N_1 is basically constant for Z ⟩ 800 (KDF = 0.6) but depends on Z if the minimum local buckling load N_{min} is chosen as a design load. The minimum local buckling load SPLA curve is lower compared to the LRSM and SBPA curves for $Z > 800$.

The experimental results of the IW1 test series can be approximated very well with the LRSM and the SBPA curves except for one test case (IW1–16) which probably buckled in the plastic range and the former design curves were developed for pure elastic buckling, which explains the discrepancy in this case. The SPLA design curve for N_1 is not conservative with respect to the experimental results but the curve corresponding to N_{min} is well below the test series.

The relative slenderness λ curves for different geometric ratios were calculated using the LRSM for an isotropic and unstiffened cylinder with clamped boundary conditions at both edges and are shown in Fig. 13 (right). This is an early look at the design curves which are currently under development. The LRSM delivers in this case conservative estimation of all experimental results and reveals quite different design lower-bounds for different L/R ratios, note that currently in engineering design empirical lower-bounds are used meaning one lower-bound "undercutting" all experimental results but not considering the individual geometric ratios of the shells. There is a lot of potential to be unveiled.

3.4. Summary

In this chapter a benchmark example was defined in order to show the challenges of shell buckling design. The present test series consisted of 33 nominal identical steel cylinders which have an average buckling KDF of 0.5 (minimum KDF = 0.4). The initial geometric imperfections where measured and approximated using a double Fourier series. The analytical solution for this shell results in an elastic buckling load of 7.9 kN. Numerical simulations using ABAQUS were performed in order to approximate the experimental buckling loads. GNIA using the MGI were performed however, those simulations were still far off the experimental results as shown in Fig. 14. Lower-bound concepts like the SPLA, LRSM and SBPA deliver far better approximations of the experimental test series, especially if yielding is considered. Also, when compared to the MGI approach, the presented lower-bound design concepts are relatively simple to implement in FEM codes.

4. Analysis of a wind turbine tower under combined load

4.1. Benchmark geometry and finite element model

The wind turbine tower shell is based on the international shell buckling exercise from Sadowski et al. [56,5] and is shown in Fig. 15. The tower shell is a cylindrical-conical-cylindrical shell which

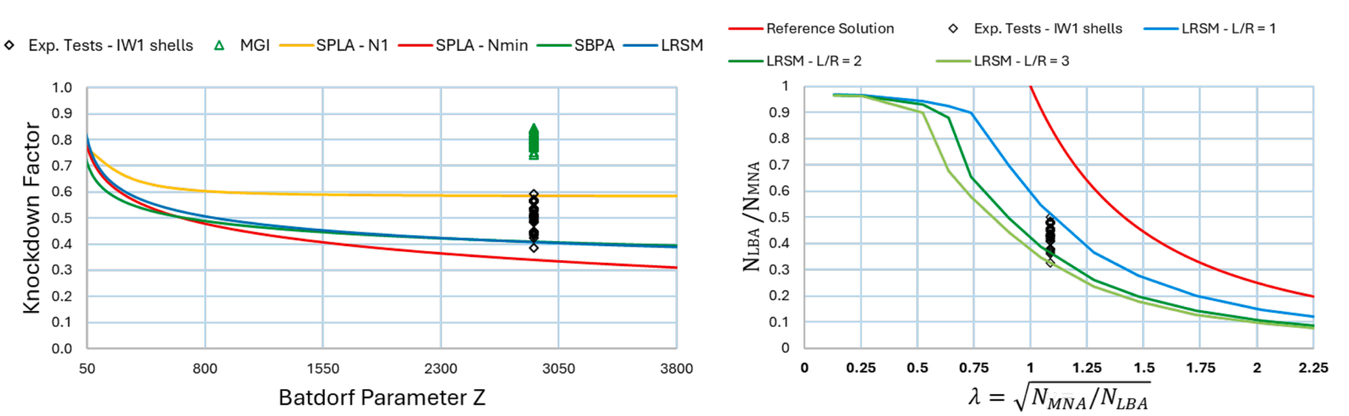

Fig. 13. Comparison of lower-bound approaches vs experiments for IW1 shells for elastic buckling (left) and plastic buckling (right).

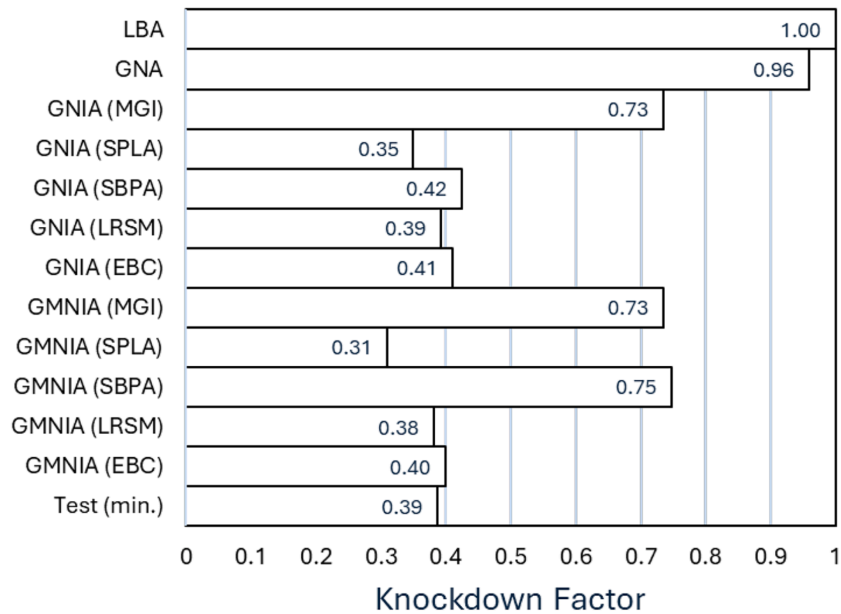

Fig. 14. Comparison of numerical analysis types vs. experiments for IW1 shells.

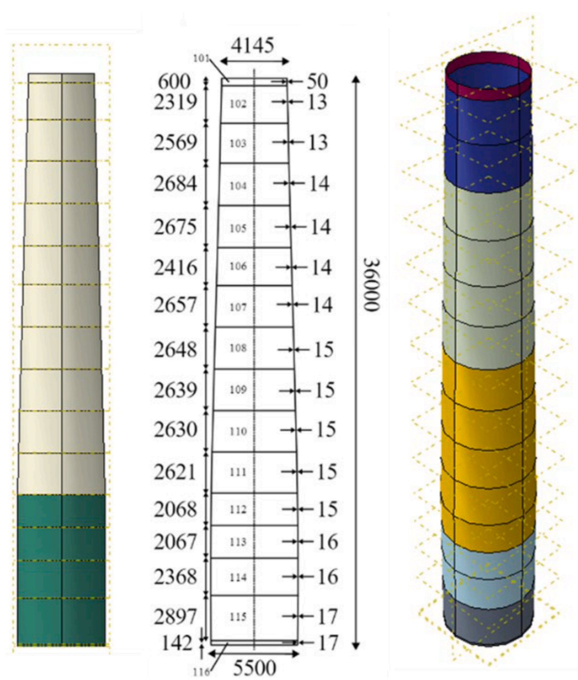

Fig. 15. Wind turbine tower geometry details: (left) main cylinder-cone transition (middle) detailed geometry (right) tower with different shell thickness sections.

transitions from a cylinder to a cone between section 110–111 and transitions back to a cylinder at the tower top, the main geometry properties and ratios of the tower are given in Table 3.

The wind turbine tower shell has a varying thickness of 17 mm at the bottom and 13 mm at the top as shown in Fig. 15. The material is S355J0 grade steel and the corresponding material properties are given in Table 3.

The tower was modeled using linear shells elements with reduced integration (S4R [59]). The mechanical boundary conditions on the bottom tower end are defined as clamped by using rigid-body interactions (Tie – in ABAQUS) which is coupled with a reference point.

Table 3
Geometry and material data for tower shell [56].

Material parameter	
elasticity modulus **E** - [MPa]	210 000
Poisson's ratio n	0.3
Yield strength Y - [MPa]	345
Density r - [kg/m^3]	7850
Geometry parameter	
Radius **R** - [mm]	2750
Cylinder Length **Lc** - [mm]	9542
Tower Length **L** - [mm]	36,000
Thickness **t** – [mm]	15
R/t	183.3
Lc/R	3.47
L/R	13.1
Z (only bottom cylinder)	2105

An additional reference point was defined at the tower top (see Fig. 16), here two points loads were defined for the vertical force and shear force, and two moments for the bending moment and the torque moment, the remaining degrees of freedom (DOF) are free. The loads originated largely from the dead weight of the rotor and the nacelle assembly [56].

The reference buckling loads for this article are determined for a perfect shell (no imperfections) and are determined according to a linear bifurcation analysis (LBA) and a material nonlinear analysis (MNA) which is based on perfect plastic material law. In addition, a geometrically and material nonlinear analysis (GMNA) combining perfect plastic material law and nonlinear large deflection theory. The multiple combined loads at the tower top are represented by a load proportionality factor (LPF) which is the ratio of the measured load divided by the design load. The tower has two load cases (LC) which are summarized in Table 4. The main difference between LC1 and LC2 is that LC2 has additional torsion.

The first eigenmodes of the LBA are shown in Fig. 16 (right), the deformation plot for LC1 indicates that the most sensitive part of the tower is the transition zone between cylinder and cone. The first eigenmode of LC2 is dominated by the deformation of the torque moment. The linear buckling LPF for LC1 equals to 3.01 (which means the tower can withstand 3 times the design load according to a linear analysis). In case of LC2 the additional torsion reduced the LPF to 1.41.

The results of the MNA and GMNA are shown in Fig. 17. The

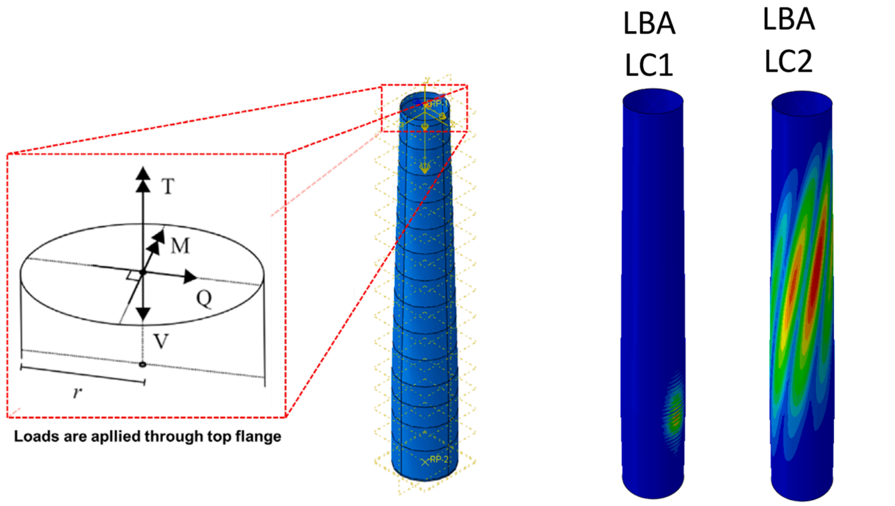

Fig. 16. Wind turbine tower loading details (left) first eigenmode of LBA for LC1 & LC2 (right).

Table 4
Loads and LPFs of the wind turbine tower for different load cases LC1 and L2.

Design loads	Load Case 1 (LC1)	Load Case 2 (LC2)
Torque moment	–	22 MNm
Shear force	1.76 MN	1.6 MN
Vertical force	4 MN	4 MN
Bending moment	33 MNm	30 MNm
Analysis type	LPF (LC1)	LPF (LC2)
LBA	3.01	1.43
MNA	1.85	1.89
GMNA	1.20	1.29

influence of yielding reduces the LPF in case of LC1 by about 40 %, the additional influence of nonlinear geometry reduces the LPF further by 36 %. As shown in Fig. 18, the slenderness ratio of the wind turbine tower indicates that plastic buckling is relevant for this analysis because $\lambda < 1$ for LC1. In the case of LC2 the LPF is 1.89 which is 32 % higher compared to the linear LPF of 1.43. The linear elastic buckling load for torque is usually much smaller than the plastic buckling load, which explains this behavior. The consideration of additional nonlinear geometry reduces the buckling LPF of LC2 to 1.29. The LPFs for both load cases are already at 1.2 / 1.29 and this is without consideration of imperfections.

4.2. Application of shell buckling design concepts to the wind turbine tower

In this section different concepts for the design of imperfection sensitive cylindrical shells are presented and applied to the wind turbine tower geometry from Section 3. The geometric imperfections which lead to the highest buckling load reduction from chapter 3, (IW1–33) were scaled to the geometry of bottom cylinder (see Fig. 19) of the wind-turbine tower and corresponding results are shown in Fig. 20.

The buckling load reduction ranges from 9 – 14 % when MGI are applied compared to the GMNA without imperfections. Within the ISBE, the tower model should represent an 'excellent' (but not perfect) construction quality which could be interpreted as "low imperfection magnitude" and low buckling load reduction as shown in Fig. 20.

The SPLA was applied next to the wind turbine tower, here two positions are of interest, the intersection between cylinder and cone and the middle of the bottom cylinder, as shown in Fig. 21. The SPLA results for the wind turbine tower (both load cases – intersection between cone and bottom cylinder) are shown in Fig. 22. The LPF corresponding to the minimum local buckling load are 0.52 for LC1 and 0.59 for LC2 for the position intersection between cone and bottom cylinder. If the perturbation load is applied to the middle of the cylinder the resulting LPF are 0.67 for LC1 and 0.71 for LC2 (20–28 % higher compared to the intersection area).

For the SPLA results there is room for interpretation because according to the requirements of the ISBE the tower model should represent an 'excellent' (but not perfect) construction quality which the

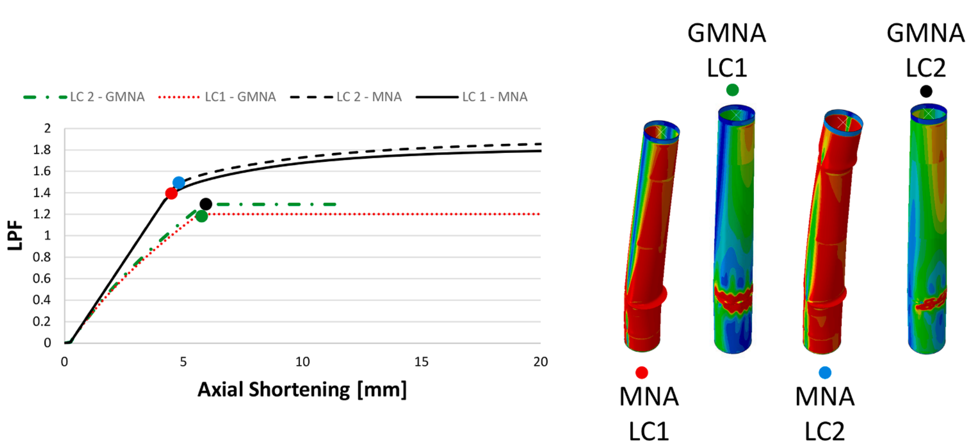

Fig. 17. LPF vs. axial shortening of the tower for MNA and GMNA (left) plots of the tower (right).

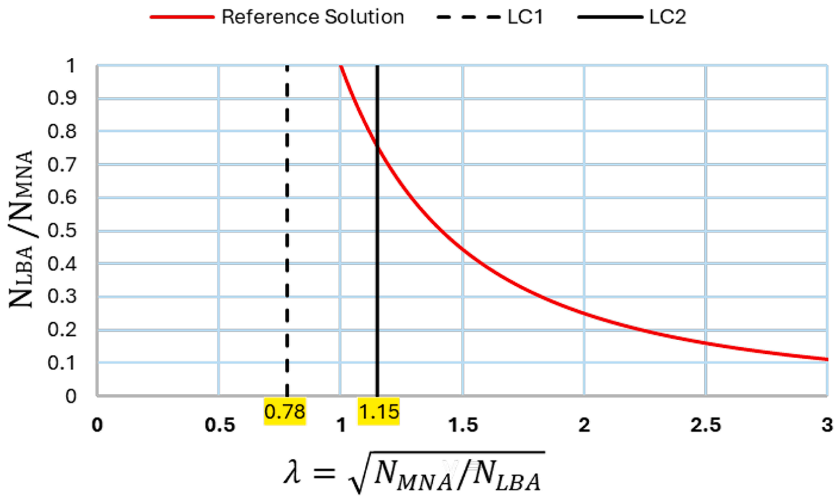

Fig. 18. LC1 and LC2 with respect to their corresponding slenderness.

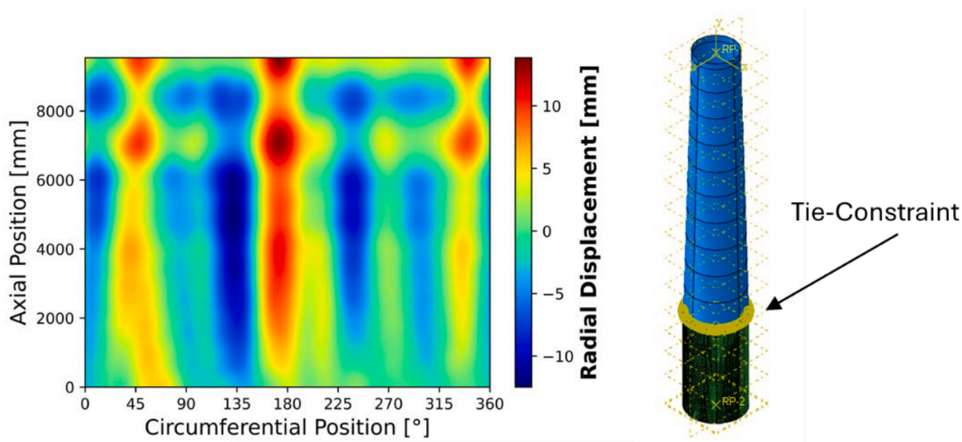

Fig. 19. Imperfection pattern for the bottom cylinder of the tower (left) numerical model of the tower with imperfect bottom cylinder (right).

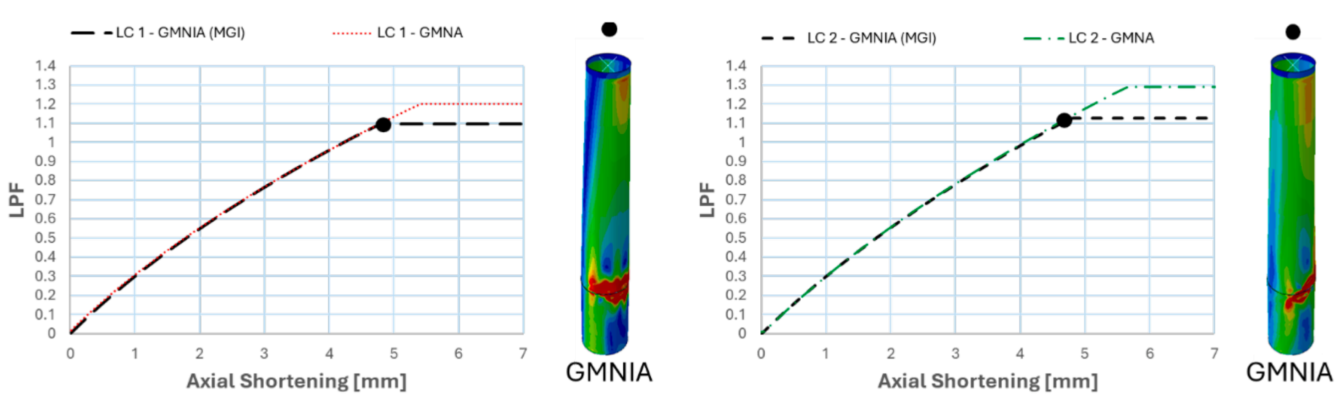

Fig. 20. LPF vs. axial shortening for the tower according to GMNIA (MGI – IW1–33): LC1 (left) LC2 (right).

authors interpret as the LPF corresponding to N_1 load of the SPLA (buckling load in the plateau range) which correspond to 0.79 for LC1 and 0.77 for LC2 for the intersection area and 0.9 for LC1 and 0.89 for LC2 for the middle of the cylinder.

The SBPA cannot be applied to the tower as it relies on the application of an edge imperfection which does not work in combination with the other loads (bending, torsion, shear), also the most sensitive part of the tower is not on the top or bottom edge but at the intersection from cylinder to cone section (section 112). In addition, as shown in Section 3 of this paper, the SBPA does overestimate the buckling load if yielding is relevant. The LRSM can in general be applied to the tower but a lower-bound cannot be found, the buckling load reduces but no plateau can be identified if the imperfection is applied and incrementally increased, as shown in Fig. 23. Usually there is a plateau for the buckling load between $0 < Rs/R < 0.4$ but not in this case.

This is most likely because only the bottom end of the tower is fixed (and not also the top end), local buckling cannot be induced using this kind of imperfection combined with the present mechanical boundary

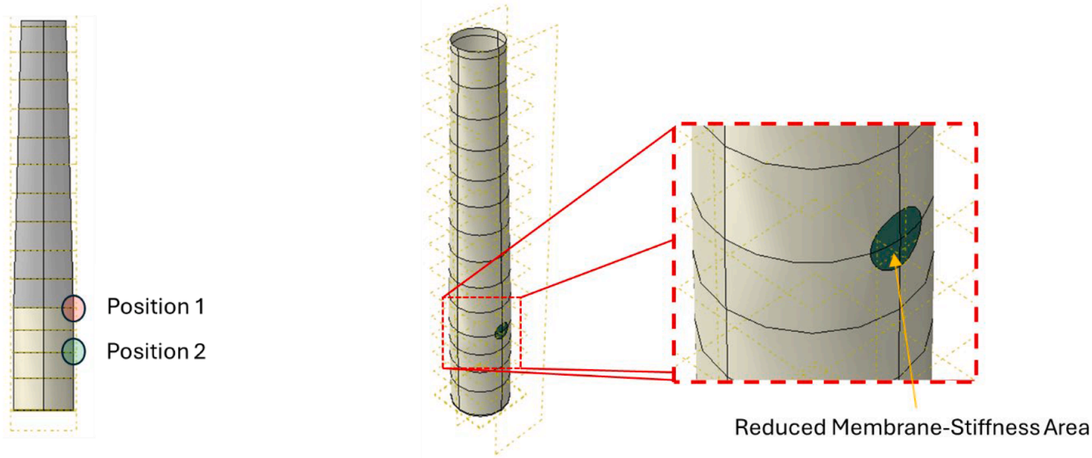

Fig. 21. Position 1 & 2 of the perturbation (EBC, LRSM & SPLA) for the tower (left) – LRSM illustration for the tower at position 1 (right).

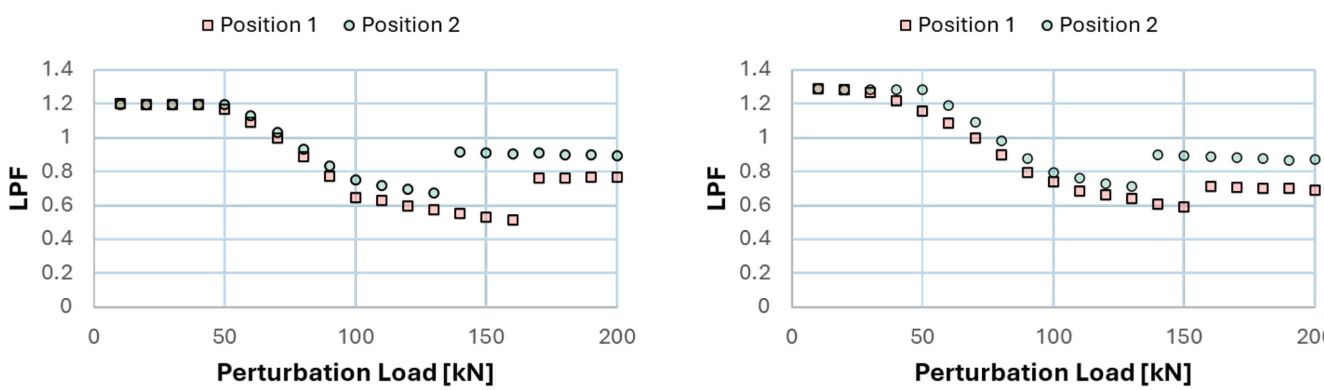

Fig. 22. SPLA diagram for the tower: LC1 (left) LC2 (right).

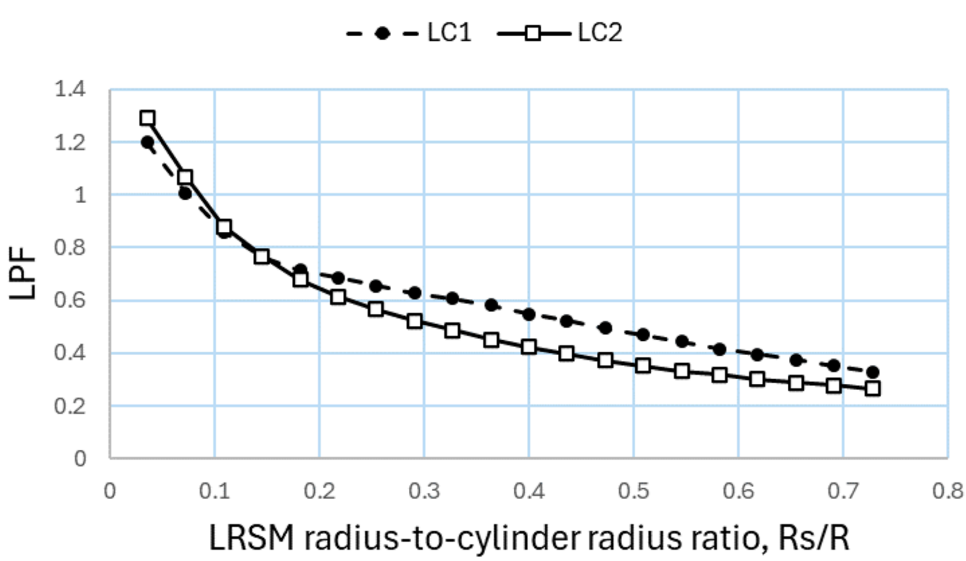

Fig. 23. LRSM diagram for the wind turbine tower.

conditions.

For the EBC only the intersection area between cylinder and cone was investigated, the results are shown in Fig. 24. The design LPF of the EBC corresponds to the load increment which leads to a reaction force Rf = 0 and was determined to LPF = 0.82 for both load cases. In the case of the EBC the 'excellent' (but not perfect) construction quality is not applicable.

4.3. *Application of analytical knockdown factors to the wind turbine tower*

In this section the EBC results for the wind turbine tower with its

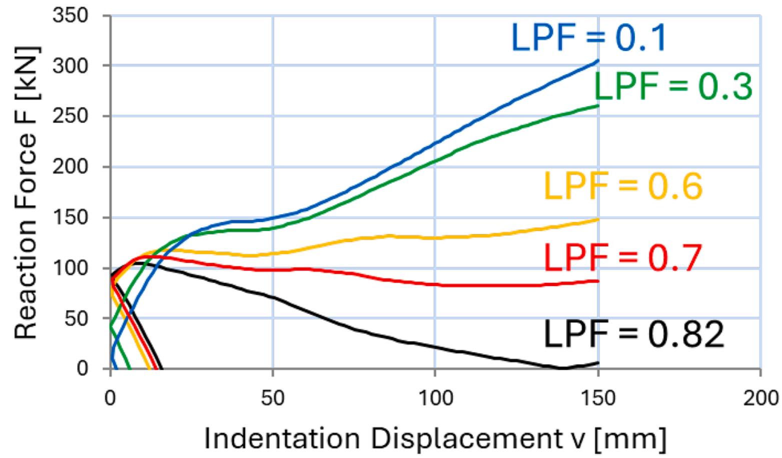

Fig. 24. EBC diagram for the tower.

combined loads are compared with analytical KDFs for cylinders under axial compression (for pure elastic buckling) in Fig. 25 (left). For this analysis only the bottom cylinder was considered as it is assumed that it is the most sensitive part of the tower. For LC1 the KDFs are not applicable because the tower is well in the plastic buckling range, the KDFs overestimate the buckling capacity. For LC2 the KDFs underestimate the buckling capacity.

A more accurate approach is to look at the relative slenderness ratio λ because it considers the material behavior (elastic or plastic buckling). The EBC was used to determine design curves for cylinder under axial compression and for the tower with its combined load cases. Note, that the results shown in Fig. 25 (right) are still at an early stage and not yet ready for all geometric configurations, the slenderness curves depend on R/t and L/R ratio and require a large amount of calculations. Also, they are not the focus of this article but still important for the estimation of the tower buckling capacity in a future design scenario.

This comparison highlights significant limitations in the current application of design curves in engineering practice, the design curves for an isotropic cylinder:

1. uniform thickness
2. under axial compression
3. With both edges clamped

Are used for a wind turbine tower:

1. Non-uniform thickness
2. Under axial compression, bending, shear and torsion
3. Only bottom edge is fixed
4. Whole tower or only a section of the tower?

The bottom cylinder has $L/R = 3.47$ and $R/t = 183$ which means the approximate design values should be between the green and blue EBC curves. The exact design curves according to the EBC have been also determined partially (7 points – to show a general trend) and plotted in Fig. 25 (right). For LC1 the EBC cylinder curves overestimate the EBC tower capacity for LC2 the EBC cylinder curves underestimate the EBC tower capacity. This example shows that with the increasing number of wind turbine towers being built, a revision of corresponding design codes seems to be in dire need.

4.4. Summary

The summarized results for the wind turbine tower with the two load cases are shown in Fig. 26. The results indicate that the additional torque moment for LC2 does not really influence the buckling loads as both LPF are the same for the GMNIA (with MGI). In Addition, the results show that the design loads of the tower are not safe as they are about 20 % lower in the case of the EBC and 25 % lower in the case of the SPLA compared to LPF = 1.0 although it was stated in the exercise that partial safety factors are already included in the design. It can be concluded that there is a definitive need for more research regarding firstly the application of dimple imperfection concepts to wind turbine towers and problems with plastic buckling in general.

5. Conclusion and outlook

This article is a follow-up article to the results of the international

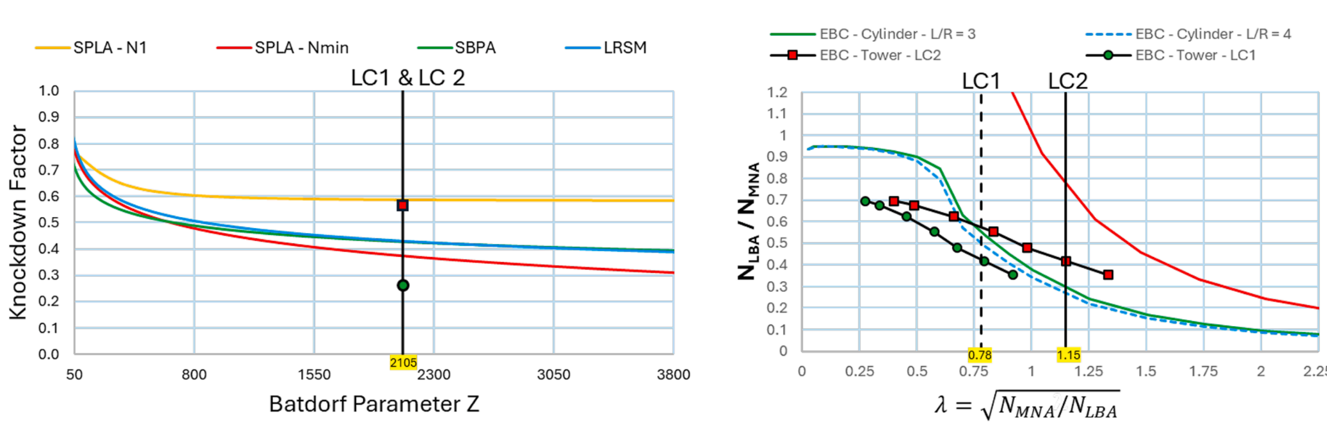

Fig. 25. Summary of results for the different analysis types for the wind turbine tower and both load cases.

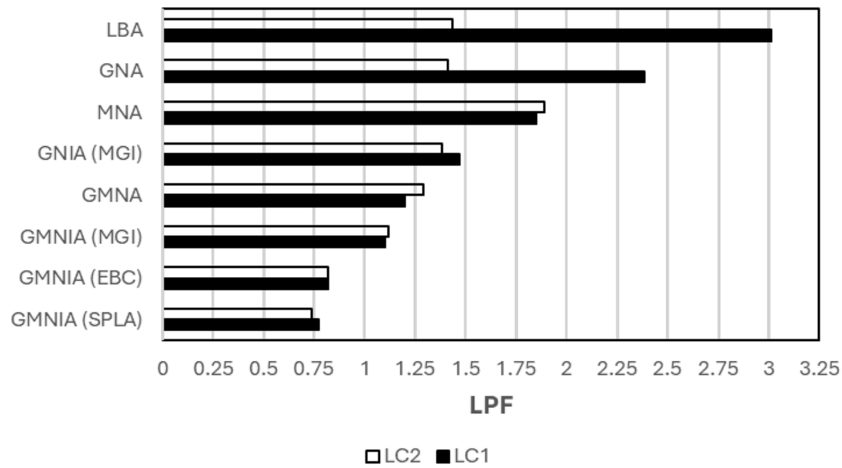

Fig. 26. Summary of results for the different analysis types for the wind turbine tower and both load cases.

shell buckling exercise (ISBE) which are published in [56]. The main tasks of this article are to simplify and summarizes the results of the ISBE in chapter 2 to increase the research audience and to show how the authors which participated in the ISBE overcome its challenges.

Shell buckling is one of the main challenges for wind turbine tower design and strangely enough, the wind turbine tower design still relies on ancient imperfection concepts like eigenmode imperfections which is clear from the ISBE.

For the demonstration of state-of-the-art imperfection concepts the authors of this article defined a simple to reproduce example in chapter 3 and discussed the limits of applicability of the dimple concepts. In chapter 4, the wind turbine tower was analyzed using the lessons learned from chapter 3. In comparison to the eigenmode imperfections, the presented EBC and SPLA deliver a definitive design value for the buckling load and are easy to realizes in modern FEA codes like ABAQUS. This results also show that the proposed design values of the wind turbine tower are not conservative enough because the design loads of the EBC/SPLA are about 20 % lower.

For future research, we identified the following topics:

1. Application of dimple imperfection concepts for elastic and plastic buckling, some concepts (LRSM) work better than others (SBPA) for elastic and plastic buckling, why is that in detail?
2. The relative slenderness λ depends on geometric ratios R/t and L/R and should be computed in dependence on those ratios
3. The relative slenderness λ depends on the applied load cases and should be computed for different load cases
4. Based on the results in Section 4, it seems that the influence of imperfections or local snap-through buckling is reduced in the plastic buckling range, is it really like this?
5. Based on the results in Section 4, could a specific design approach (EBC or SPLA) be proposed for wind turbine towers under certain structural configurations and load conditions?

Author agreement statement

We the undersigned declare that this manuscript is original, has not been published before and is not currently being considered for publication elsewhere.

We confirm that the manuscript has been read and approved by all named authors and that there are no other persons who satisfied the criteria for authorship but are not listed. We further confirm that the order of authors listed in the manuscript has been approved by all of us.

We understand that the Corresponding Author is the sole contact for the Editorial process. He/she is responsible for communicating with the other authors about progress, submissions of revisions and final approval of proofs

CRediT authorship contribution statement

H.N.R. Wagner: Writing – review & editing, Writing – original draft, Validation, Software, Methodology, Investigation, Formal analysis, Data curation, Conceptualization. **C. Hühne:** Supervision, Software, Resources, Funding acquisition.

Declaration of competing interest

The authors declare that they have no known competing financial interests or personal relationships that could have appeared to influence the work reported in this paper.

Appendix

This chapter summarizes the Eqs. (6) – (9) for SPLA N1, SPLA Nmin, SBPA [61] and LRSM [50] in terms of the Batdorf Parameter Z from Fig. 27. The equations are considered valid for $50 < Z < 5000$.

$$\rho_{SPLA-N_1} = 0.5830967 + \frac{0.7790791 - 0.5830967}{1 + \left(\frac{Z}{235.9102}\right)^{1.751103}} \tag{6}$$

$$\rho_{SPLA-min} = -551.8718 + \frac{552.8144 - -551.8718}{1 + \left(\frac{Z}{858.6543}\right)^{0.0003917715}} \tag{7}$$

$$\rho_{SBPA} = 1.23 \cdot Z^{-0.138} \tag{8}$$

$$\rho_{LRSM} = 1.58 \cdot Z^{-0.17} \tag{9}$$

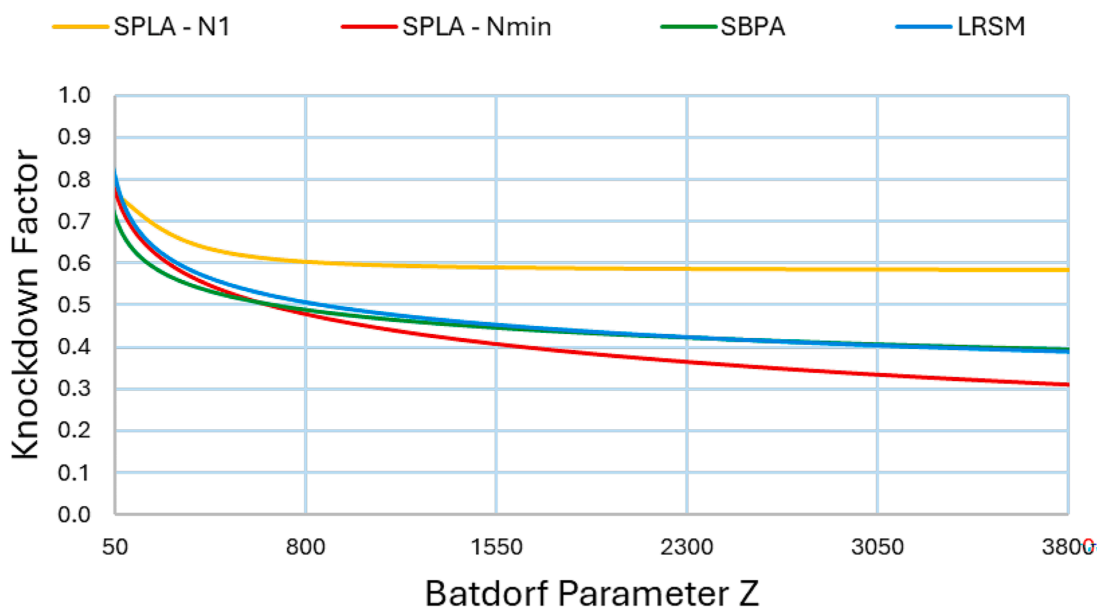

Fig. 27. Lower-Bound Curves for cylinder under axial compression according to different dimple concepts.

Data availability

The data will be uploaded to Github.

References

[1] M.W. Hilburger, W.A.J. Waters, W.T. Haynie, Buckling test results from the 8-foot-diameter orthogrid-stiffened cylinder test article TA01. [Test Dates: 19-21 November 2008] l-20490, (2015) NF1676L–20067.

[2] H. Wagner, C. Hühne, S. Niemann, Buckling of launch-vehicle cylinders under axial compression: a comparison of experimental and numerical knockdown factors, Thin-Walled Struct. 155 (2020) 106931, https://doi.org/10.1016/j.tws.2020.106931.

[3] J. Zhang, Y. Wang, F. Wang and W. Tang, "Buckling of stainless steel spherical caps subjected to uniform external pressure".*Ships Offshore Structu.*10.1080/17445302.2018.1459358.

[4] H. Wagner, G. Niewöhner, A. Pototzky, C. Hühne, On the imperfection sensitivity and design of tori-spherical shells under external pressure, Internat. J. Press. Vessels Pip. 191 (2021) 104321, https://doi.org/10.1016/j.ijpvp.2021.104321.

[5] A. Sadowski, M. Seidel, 8-MW wind turbine tower computational shell buckling benchmark. Part 2: detailed reference solution, Eng. Fail. Anal. 148 (2023).

[6] H. Ali, H. Wagner, C. Akalın, I. Tabrizi, C. Hühne, M. Yildiz, Buckling and fracture analysis of thick and long composite cylinders with cutouts under axial Compression: an experimental and numerical campaign, Compos. Struct. 324 (2023) 117530, https://doi.org/10.1016/j.compstruct.2023.117530.

[7] H. Wagner, C. Hühne, R. Khakimova, On the development of shell buckling knockdown factors for imperfection sensitive conical shells under pure bending, Thin-Walled Struct. 145 (December 2019) 106373.

[8] ECCS, Buckling of Steel shells: European design recommendations, 5th ed, 5th Edition, European Convention for Costructional Steelwork, 2008.

[9] S.G. Castro, R. Zimmermann, M.A. Arbelo, R. Khakimova, M.W. Hilburger, R. Degenhardt, Geometric imperfections and lower-bound methods used to calculate knock-down factors for axially compressed composite cylindrical shells, Thin-Walled Struct. 74 (2014) 118–132.

[10] A. Meurer, B. Kriegesmann, M. Dannert, R. Rolfes, Probabilistic perturbation load approach for designing axially compressed cylindrical shells, Thin-Walled Struct. 107 (2016) 648–656.

[11] B. Kriegesmann, M. Hilburger, R. Rolfes, The effects of geometric and loading imperfections on the response and lower-bound buckling load of a compression-loaded cylindrical shell, in: 53rd AIAA/ASME/ASCE/AHS/ASC Structures, structural dynamics and materials conference, 2012.

[12] W.T. Koiter, The stability of elastic equilibrium *[PhD thesis] - 1945 [in Dutch],* TH Delft. Englisch Translation NASA TTF-10, 1967, pp. 1–833.

[13] J.P. Peterson, P. Seide and V.I. Weingarten, "Buckling of thin-walled circular cylinders - NASA SP-8007," *Technical Report,* 1 Aug 1968.

[14] V.I. Weingarten, E.J. Morgan, P. Seide, Elastic stability of thin-walled cylindrical and conical shells under axial compression, AIAA J. 3 (1965) 500–505.

[15] H. Wagner, C. Hühne, I. Elishakoff, Probabilistic and deterministic lower-bound design benchmarks for cylindrical shells under axial compression, Thin-Walled Struct. 146 (January 2020) 106451.

[16] L. Wullschleger, H.R. Meyer-Piening, Buckling of geometrically imperfect cylindrical shells - definition of a buckling load, Int. J. Non. Linear. Mech. 37 (2002) 645–657.

[17] J. Arbocz, H. Abramovich, The initial imperfection data bank at the delft university of technology part 1, Department of aerospace engineering, LR-290, Delft University of technology, 1979.

[18] B. Kriegesmann, R. Rolfes, C. Hühne, J. Teßmer, J. Arbocz, Probabilistic design of axially compressed composite cylinders with geometric and loading imperfections, Internat. J. Struct. Stabil. Dyn. 10 (2010) 623–644.

[19] A. Takano, Statistical knockdown factors of buckling anisotropic cylinder under axial compression, J. Appl. Mech. 79 (79) (2012), https://doi.org/10.1115/1.4006450.051004.

[20] M. Fina, P. Weber, W. Wagner, Polymorphic uncertainty modeling for the simulation of geometric imperfections in probabilistic design of cylindrical shells, Struct. Safet. 82 (2020).

[21] M.W. Hilburger, "On the development of shell buckling knockdown factors for stiffened metallic launch vehicle cylinders," *2018 AIAA/ASCE/AHS/ASC Structures, structural dynamics, and materials conference*.

[22] B. Wang, S. Zhu, P. Hao, X. Bi, K. Du, B. Chen, X. Ma and Y. Chao, "Buckling of quasi-perfect cylindrical shell under axial compression: a combined experimental and numerical investigation," *Int. J. Solids. Struct.; In Press, Accepted Manuscript;* .2024.

[23] J. Kepple, M. Herath, G. Pearce, B. Prusty, R. Thomson, R. Degenhard, Stochastic analysis of imperfections sensitive unstiffened composite cylinder using realistic imperfections models, Compos. Struct. 126 (2015) 159–173.

[24] C. Schillo, D. Röstermundt, D. Krause, Experimental and numerical study on the influence of imperfections on the buckling load of unstiffened CFRP shells, Compos. Struct. 131 (1 November 2015) 128–138.

[25] F. Franzoni, Predicting buckling from vibration: an analytical, numerical, and experimental verification for cylindrical shells, Universität Bremen, 2020. Dissertation.

[26] R. Degenhardt, A. Bethge, A. Kling, R. Zimmermann, K. Rohwer, Probabilistic approach for improved buckling knock-down factors of CFRP cylindrical shells, in: Proceeding of 18th Engineering mechanics division conference, 2007.

[27] R. Khakimova, S. Castro, D.R.K. Wilckens, R. Degenhardt, Buckling of axially compressed CFRP cylinders with and without additional lateral load: experimental and numerical investigation, Thin-Walled Struct. 119 (2017) 178–189.

[28] K. Tian, B. Wang, P. Hao, A. Waas, A high-fidelity approximate model for determining lower-bound buckling loads for stiffened shells, In Internat. J. Solids Struct. (2017), https://doi.org/10.1016/j.ijsolstr.2017.10.034. *ISSN 0020-7683*.

[29] J.H.J. Starnes, M.W. Hilburger and M.P. Nemeth, "The Effects of initial imperfections on the buckling of," *Composite structures - theory and practice, P.Grant and* C. Q.Rousseau, eds., ASTM STP 1383, pp. 529–550, 2000.

[30] M.R. Schultz, D.W. Sleight, D.E. Myers, W.A. Waters, P.B. Chunchu, A.W. Lovejoy, M.W. Hilburger, Buckling design and imperfection sensitivity of sandwich composite launch-vehicle shell structures, in: Conference: Proceedings of the american society for composites: thirty-first technical conference, At Williamsburg, VA, 2016.

[31] B. Wang, K. Du, H. Peng, K. Tian, Y. Chai, L. Jiang, S. Xu, X. Zhang, Experimental validation of cylindrical shells under axial compression for improved knockdown factors, Int. J. Solids. Struct. (2019) *accepted manuscript*.

[32] M. Tillotson-Rudd, M.R. Schultz, N.W. Gardner, C.J.R. Kosztowny, C. Bisagni, Experimental validation of the buckling behavior of unreinforced and reinforced composite conical-cylindrical shells for launch-vehicles, Compos. Struct. 118493 (2024) 349–350, https://doi.org/10.1016/j.compstruct.2024.118493.

[33] H. Ma, P. Jiao, H. Li, Z. Cheng, Z. Chen, Buckling analyses of thin-walled cylindrical shells subjected to multi-region localized axial compression: experimental and numerical study, Thin-Walled Struct. 183 (2023), https://doi.org/10.1016/j.tws.2022.110330.

[34] P. Jiao, Z. Chen, H. Ma, H. Miao, H. Ou, Buckling behavior analysis of thin-walled cylindrical shell structure under localized axial compression load based on initial imperfection sensitivity, Internat. J. Struct. Stab. Dyn. 23 (2023), https://doi.org/10.1142/S0219455423501973.

[35] P. Jiao, Z. Chen, H. Ma, P. Ge, Buckling behaviors of thin-walled cylindrical shells under localized axial compression loads, Part 1: experimental study, Thin-Walled Struct. 166 (2021), https://doi.org/10.1016/j.tws.2021.108118.

[36] P. Jiao, Z. Chen, H. Ma, P. Ge, Y. Gu, H. Miao, Buckling behaviors of thin-walled cylindrical shells under localized axial compression loads, Part 2: numerical study, Thin-Walled Struct. 169 (2021), https://doi.org/10.1016/j.tws.2021.108330.

[37] I. Balbin, C. Bisagni, M. Schultz and M. Hilburger, "Scaling Methodolgy for buckling of sandwich composite cylindrical structures," *2018 AIAA/ASCE/AHS/ASC structures, structural dynamics, and materials conference, AIAA SciTech Forum, (AIAA 2018-1693)*.

[38] M.W. Hilburger, W.T. Haynie, A.E. Lovejoy, M.G. Roberts, J.P. Norris, W.A. Waters and H.M. Herring, "Subscale and full-scale testing of buckling-critical launch vehicle shell structures," *AIAA Paper 2012-1688, NF1676L-13284*.

[39] H. Wagner, H. Koeke, S. Dähne, C. Hühne, R. Khakimova, Decision tree-based machine learning to optimize the laminate stacking of composite cylinders for maximum buckling load and minimum imperfection sensitivity, Compos. Struct. 220 (15 July 2019) 45–63.

[40] H. Wagner, E. Petersen, R. Khakimova, C. Hühne, Buckling analysis of an imperfection-insensitive hybrid composite cylinder under axial compression – numerical simulation, destructive and non-destructive experimental testing, Compos. Struct. 225 (1 October 2019) 111152.

[41] M. Deml, W. Wunderlich, Direct evaluation of the 'worst' imperfection shape in shell buckling, Comput. Methods Appl. Mech. 149 (1997) 201–222.

[42] T. Winterstetter, H. Schmidt, Stability of circular cylindrical steel shells under combined loading, Thin-Walled Struct. 40 (2002) 893–910.

[43] J. Horak, J.G. Lord, M. Peletier, Cylinder buckling: the mountain pass as an organizing center, SIAM. J. Appl. Math. 66 (5) (2006) 1793–1824.

[44] C. Hühne, R. Rolfes, E. Breitbach, J. Teßmer, Robust design of composite cylindrical shells under axial compression — Simulation and validation, Thin-Walled Struct. 46 (2008) 947–962.

[45] R. Degenhardt, R. Zimmermann, A. Kling, D. Wilckens, New robust design guideline for imperfection sensitive composite launcher structures, in: 3rd CEAS Congress, Venice, Italy, 2011.

[46] P. Hao, B. Wang, G. Li, Z. Meng, K. Tian, D. Zeng, X. Tang, Worst multiple perturbation load approach of stiffened shells with and without cutouts for improved knockdown factors, Thin-Walled Struct. 82 (2014) 321–330, https://doi.org/10.1016/j.tws.2014.05.004.

[47] B. Wang, P. Hao, G. Li, Y. Fang, X. Wang, X. Zhang, Determination of realistic worst imperfection for cylindrical shells using surrogate model, Struct. Multidisciplin. Optimiz. 48 (2013) 777–794.

[48] H. Wagner, C. Hühne, Robust knockdown factors for the design of cylindrical shells under axial compression: potentials, practical application and reliability analysis, Int. J. Mech. Sci. 135 (2018) 410–430.

[49] H. Wagner, C. Hühne, S. Niemann, Robust knockdown factors for the design of axially loaded cylindrical and conical composite shells - Development and Validation, Compos. Struct. 173 (2017) 281–303, https://doi.org/10.1016/j.compstruct.2017.02.031.

[50] H. Wagner, E. Sosa, C. Hühne, T. Ludwig, J. Croll, Robust design of imperfection sensitive thin-walled shells under axial compression, bending or external pressure, Int. J. Mech. Sci. 156 (2019) 205–220.

[51] H. Wagner, C. Hühne, J. Zhang, W. Tang, On the imperfection sensitivity and design of spherical domes under external pressure, Internat. J. Press. Vessels Pip. 179 (2020).

[52] J. Croll, Towards a rationally based elastic-plastic shell buckling design, Thin-Walled Struct. 23 (1995) 67–84.

[53] J. Croll, R. Batista, Explicit lower bounds for the buckling of axially loaded cylinders, Int. J. Mech. Sci. 23 (1981) 333–343.

[54] H. Wagner, C. Hühne, J. Zhang, W. Tang, R. Khakimova, Geometric imperfection and lower-bound analysis of spherical shells under external pressure, Thin-Walled Struct. 143 (October 2019) 106195.

[55] H. Wagner, C.R.K. Hühne, Towards robust knockdown factors for the design of conical shells under axial compression, Int. J. Mech. Sci. 146-147 (2018) 60–80.

[56] A. Sadowski, M. Seidel, P. Zhang, H. Wagner, H. Karampour, A. Fischer, C. Fischer, F. Marthen, S. Mishra, L. Chen, 8-MW wind turbine tower computational shell buckling benchmark. Part 1: an international 'round-robin' exercise, Eng. Fail. Anal. 148 (2023).

[57] B. Wang, K. Du, P. Hao, C. Zhou, K. Tian, S. Xu, Y. Ma, X. Zhang, Numerically and experimentally predicted knockdown factors for stiffened shells under axial compression, Thin-Walled Struct. 109 (2016) 13–24, https://doi.org/10.1016/j.tws.2016.09.008.

[58] W. Verduyn, I. Elishakoff, A testing machine for statiscial analysis of small imperfect shells: Part 1, Delft University of Technology, Department of Aerospace Engineering, Delft, Netherlands, 1982.

[59] Dassault Systems, ABAQUS 6.13—Software Package, 2013.

[60] R. Groh, A. Pirrera, On the role of localizations in buckling of axially compressed cylinders, Proc. R. Soc. A 475 (2019), https://doi.org/10.1098/rspa.2019.0006.

[61] A. Evkin, V. Krasovsky, O. Lykhachova, V. Marchenko, Local buckling of axially compressed cylindrical shells with different boundary conditions, Thin-Walled Struct. 141 (August 2019) 374–388.

[62] H. Wagner, C. Hühne, K. Rohwer, S. Niemann, M. Wiedemann, Stimulating the realistic worst case buckling scenario of axially compressed cylindrical composite shells, Compos. Struct. 160 (2017) 1095–1104.

[63] H. Wagner, C. Hühne, S. Niemann, Constant single-buckle imperfection principle to determine a lower bound for the buckling load of unstiffened composite cylinders under axial compression, Compos. Struct. 139 (2016) 120–129.

[64] H. Wagner, C. Hühne, M. Janssen, Buckling of cylindrical shells under axial compression with loading imperfections: an experimental and numerical campaign on low knockdown factors, Thin-Walled Struct. 151 (2020).

[65] S. Eggwertz, L. Samuelson, Buckling strength of spherical shells, J. Constr. Steel. Res. 17 (3) (1990) 195–216.

[66] H. Wagner, S.Niemann Hühne, R. Khakimova, Robust design criterion for axially loaded cylindrical shells - Simulation and Validation, Thin-Walled Struct. 115 (2017) 154–162, https://doi.org/10.1016/j.tws.2016.12.017.